IRIS AperTO

UNIVERSITÀ DEGLI STUDI DI TORINO

AperTO - Archivio Istituzionale Open Access dell'Università di Torino

Beyond TiO2: Cerium-Doped Zinc Oxide as a New Photocatalyst for the Photodegradation of Persistent Pollutants

This is the author's manuscript

Original Citation:

Availability:

This version is available http://hdl.handle.net/2318/1622513 since 2017-05-24T15:43:31Z

Published version:

DOI:10.1002/slct.201600645

Terms of use:

Open Access

Anyone can freely access the full text of works made available as "Open Access". Works made available under a Creative Commons license can be used according to the terms and conditions of said license. Use of all other works requires consent of the right holder (author or publisher) if not exempted from copyright protection by the applicable law.

(Article begins on next page)

07 October 2026

IRIS AperTO

UNIVERSITÀ DEGLI STUDI DI TORINO

This is the author's final version of the contribution published as:

Paganini, Maria Cristina; Dalmasso, Daniele; Gionco, Chiara; Polliotto, Valeria; Mantilleri, Lorenzo; Calza, Paola. Beyond TiO2: Cerium-Doped Zinc Oxide as a New Photocatalyst for the Photodegradation of Persistent Pollutants. CHEMISTRYSELECT. 1 (12) pp: 3377-3383.
DOI: 10.1002/slct.201600645

The publisher's version is available at:
http://onlinelibrary.wiley.com/wol1/doi/10.1002/slct.201600645/fullpdf

When citing, please refer to the published version.

Link to this full text:
http://hdl.handle.net/2318/1622513

This full text was downloaded from iris - AperTO: https://iris.unito.it/

iris - AperTO

University of Turin's Institutional Research Information System and Open Access Institutional Repository

Beyond TiO_2: cerium doped zinc oxide as new photocatalyst for the photodegradationof persistent pollutants.

M.C. Paganini, D. Dalmasso, C. Gionco, V. Polliotto, L. Mantilleri, P. Calza*

Abstract: We prepared via hydrothermal synthesis zinc oxide samples doped with cerium. The samples were characterized via powder X Ray Diffraction measurements, Diffuse Reflectance UV Vis spectroscopy, Scanning Electron Microscopy and Transmission Electron Microscopy with EDX (Energy Dispersive X-Ray spectroscopy) analysis, and BET (Brunauer–Emmett–Teller) surface area analysis. XRD measurements reveal the formation of highly crystalline materials; wurtzite is the most important.

All materials were tested using phenol as model molecule and their performances were compared with TiO_2 P25. The material showing the best performance, namely Ce-doped ZnO, was then used to abate some emerging pollutants. We chose three iodinated X-ray contrast agent (ICM), iopromide, iopamidol and diatrizoate, known to be recalcitrant to traditional advanced oxidation processes. In the presence of TiO_2 P25, all ICM exhibited a slow degradation, with $t_{1/2}$ ranging from 30 min (iopamidol) to 120 min (diatrizoate) and several hours are required for their complete disappearance. The employment of Ce-doped ZnO leads to a sharp increase in their disappearance, with $t_{1/2}$ obtained within 15 min (iopamidol) or 25 min (diatrizoate) and the complete abatement is achieved within 2h.

Introduction

Metal oxides semiconductors such as TiO_2, ZnO, WO_3 etc. have been attempted for the photocatalytic degradation of a wide variety of environmental contaminants. Heterogeneous photocatalysis based on nano-structured TiO_2 has been extensively studied as an important destructive technology leading to the total mineralization of a wide range of organic dyes. In some cases, ZnO exhibits a better photocatalytic efficiency than TiO_2, but only few works reported that the photocatalytic activity of ZnO is better than Degussa P25 titania (P25), [1] which has been proved to be one of the most efficient photocatalysts, and widely used as a benchmark. However, both TiO_2 and ZnO are activated only under UV irradiation because of their large band gap (3.2 and 3.4 eV respectively), which greatly limits their application in environmental decontamination as solar spectra only contain 5% of UV. Therefore, it is crucial to explore efficient methods to extend their photocatalytic response from UV to visible region. Previous papers by some of us demonstrated that it is possible, through the dispersion of small amounts of cerium ions within the matrix of different oxides (namely zirconium dioxide or zinc oxide), to modify the photoactivity of the final material. Thereby, the modified oxide becomes photoactive in visible light and much more active in UV light. [2, 3] In the case of zinc oxide the cerium does not enter into the structure forming a solid solution due to the deep difference in dimensions of the two metal ions, but segregates as cerium oxide. The interaction between the interfaces of the two oxides is the reason of the increased photocatalytic activity. Doped zinc oxide is a promising candidate as a photocatalytic material since it demonstrates high photocatalytic efficiencies for the degradation of organic pollutants and can be a suitable alternative to TiO_2 thanks to its very similar band gap and to the different morphologies in which it can be prepared.[4, 5]. Indeed very recently, some papers have been published about Ce-doped ZnO nanostructures used for photocatalytic applications, but in that case the photoactivity was not compared with TiO_2 P25 due to the fact that it was still less efficient.[6].

In a previous paper [3] we prepared pure and doped ZnO with low cerium loading (1% molar) via hydrothermal process, a low temperature, green and simple process to obtain controlled nanostructures, starting from acetate precursor using different Cerium precursors. In the present paper, we prepared materials via the same hydrothermal method, but starting from a different zinc oxide precursor, namely zinc nitrate, that permits to obtain an increased photoactivity. We decided to mantain the low concentration of cerium (1% mol) for using this sample in comparison with the other material we already prepared [3]. The photocatalytic performance of these new materials was firstly tested on phenol and then to more refractory compounds, such as iodinated X ray contrast agents (ICM).

Prof. M.C. Paganini, Dr. D. Dalmasso, PhD. C. Gionco, Dr. V. Polliotto, Dr. L. Mantilleri, Prof. P. Calza,
Department of Chemistry
University of Turin
Via P. Giuria 5-10125 Torino-Italy
E-mail:paola.calza@unito.it

ICM, a class of medical diagnostic agents used for imaging blood vessels and organs, are among the most recalcitrant and highly persistent emerging pollutants[7]. Large quantitiesof ICM are administered to individual patients undergoing tests (>100 g dose^{-1}), and are generally excreted unmetabolized within 24 h[8]. Although often considered to be biochemically inert, some researches had shown that diatrizoate may have nephrotoxic effects in animals and humans [9].Only limited biodegradation of ICM was reported during biological wastewater treatment processes and biotransformation is very slow in soil/sediment–water incubations (e.g., $t_{1/2}$> 20 days) [10], resulting only in partial modifications to the sidechains of the core triiodinated aromatic ring structure; especially ionic ICM like diatrizoate had shown to be remarkably resistant to biotransformation [11].

Conventional drinking water treatment processes have shown as well a slight success in removing or transforming ICM [12]. Conversely, electrochemical process [13] and advanced treatment processes, i.e. UV/H_2O_2[14], UV/O_3 and O_3/H_2O_2 had shown some success in degrading ICM. Only few works explore the employment of the photocatalytic treatment with TiO_2 toward ICM; Doll and Frimmel[15] reported on the UV-TiO_2 degradation of nonionic ICM (iomeprol and iopromide), evidencing a limited mineralization. Sugihara et al. [16]studied the kinetics and mechanisms for TiO_2photocatalytic transformation of diatrizoate and structurally related compounds in both oxic and anoxic aqueous suspensions. In the present paper, we explore the possibility to treat ICM with new materials based on ZnO aimed to increase the degradation efficiency of ICM under photocatalytic treatment.

Results and Discussion

Materials characterization

XRD analysis

XRD patterns of the samples investigated in this work are shown in Figure 1. The peculiar peaks corresponding to the diffraction patterns of hexagonal wurtzite phase of ZnO are observed. The pattern of undopedZnO corresponding to (1 0 0), (0 0 2), (1 0 1), (1 0 2), (1 1 0), (1 0 3), (2 0 0), (1 1 2) and (2 0 1) planes are in accordance with the wurtzite hexagonal phase of ZnO [18].

The introduction of Cerium does not bring any modifications in the crystal structure of ZnO, but the cerium introduced as dopant in the sample segregates as CeO_2 phase as it can be seen in Figure 1, bottom; in particular the peak related to the (1 1 1) plane is observed. Moreover, in both samples some peaks, of very low intensity, related to the $NaNO_3$ phase can also be identified, being a residual from the synthesis procedure.

On the XRD patterns a Rietveld refinement was performed using the MAUD software [17]. Table 1 lists the calculated relative abundance of the two oxides, lattice parameters and average crystals size. The lattice parameters of ZnO are not influenced by the introduction of Ce. The ZnO crystallites are large (between 150 and 300nm), while the CeO_2 crystallites, obtained as segregation phase, are significantly smaller (about 10 nm).

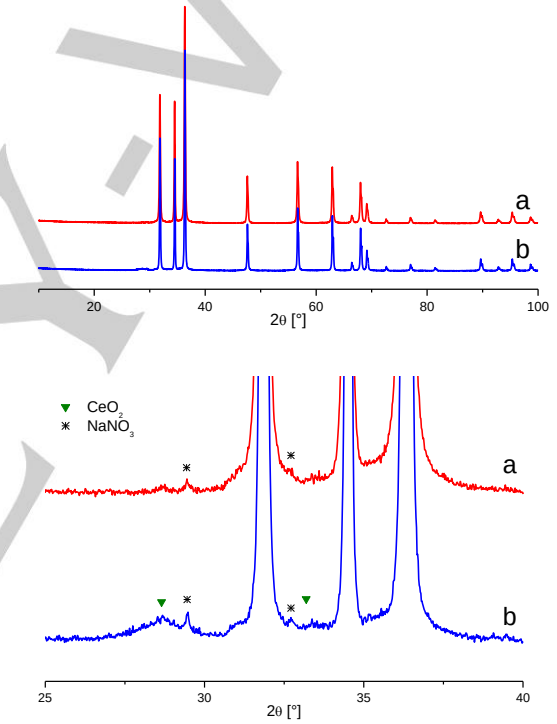

Figure 1. XRPD ptterns of ZnO (a) and Ce-ZnO (b). Top: full pattern. Bottom: Magnification of patterns.

Table 1. Cell parameters, weight and molar percentage and crystallite size obtained from Rietveld refinement of the XRD patterns of bare and doped ZnO. R_{wp} is the weighted residual error, *a* and *c* are lattice parameters, d is the average crystallite dimension.

Sample	Phase	R_{wp}	%mol	*a* [Å]	*c* [Å]	d [nm]
ZnO		9.15				
	ZnO		100%	3.252	5.210	160
Ce-ZnO		10.12				
	ZnO		99%	3.252	5.210	299
	CeO_2		1%	5.404		9

WILEY-VCH

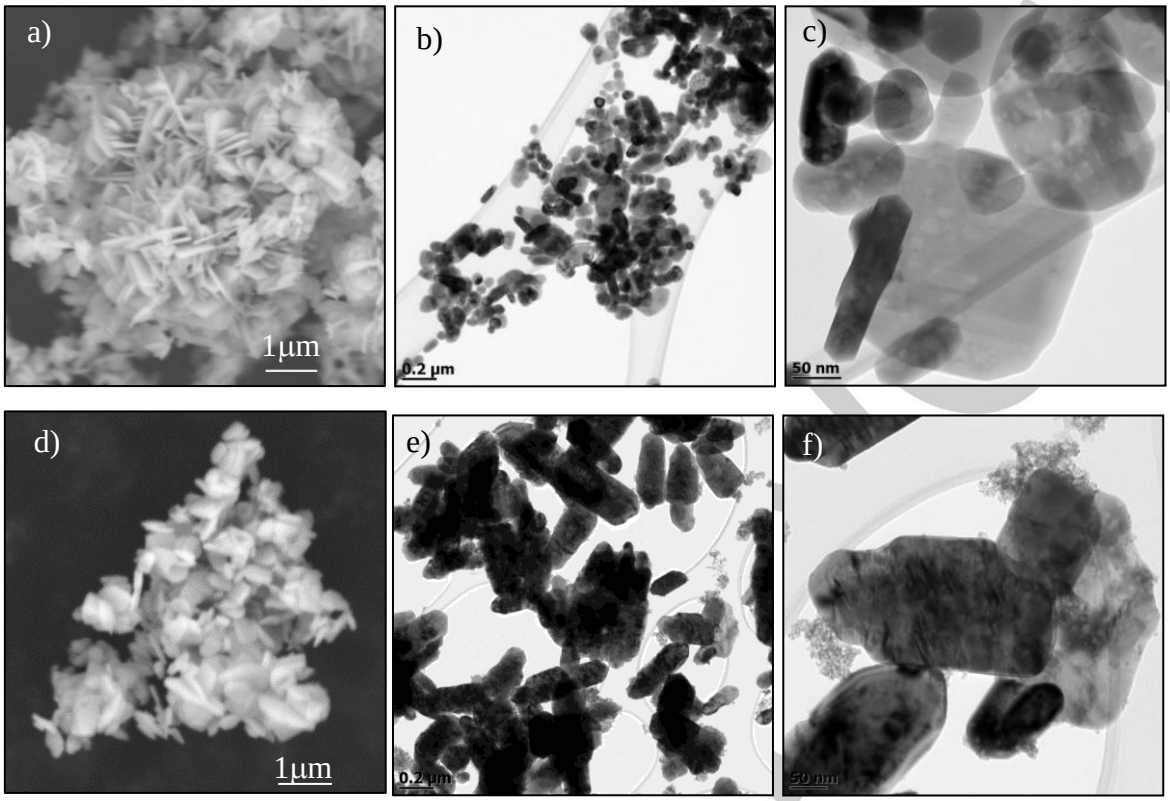

Figure 2. SEM (a, d) and TEM (b, c, e, f) images of ZnO (a, b, c) and Ce-ZnO (d, e, f).

Scanning Electron microscopy and Transmission Electron Microscopy analysis

Figure 2 depicts the surface morphology of pure ZnO (Fig. 2a, b, c) and Ce-ZnO (Fig. 2d, e, f) catalysts. The SEM images (Fig. 2 a and d) show the morphology of the particles: they look like platelets that form big aggregates. To be more specific, bare ZnO (Fig. 2a) exhibits clusters of platelets that form a sort of flower like hierarchical structure. On the other hand, the doped catalyst (Fig. 2d) with cerium chloride, revealed bigger flakes, which aggregate, leading to the formation of a cluster.

The TEM images (Fig. 2b, c, e, f), in which the particles are more dispersed than in SEM images, reveal that both catalysts present different morphologies and different dimension of particles: most of them look like large and thin platelets with different elongation according to the axes, other exhibit spherical or hexagonal plate-like shape. Ce-ZnO sample (Fig. 2 e and f) shows, for the wurtzite phase, crystals bigger than those of bare ZnO (Fig. 2 e and f), confirming the XRD results. Furthermore, the addition of Ce results in a complete segregation as little sferical particles of CeO_2, as one can deduce from the EDX map of Ce-ZnO sample, reported in Figure 3.

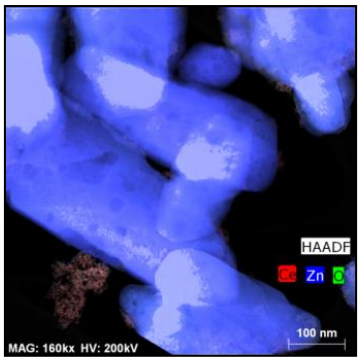

Figure 3. EDX atomic maps of Ce (red), Zn (blue) and O (green) for Ce-doped ZnO sample.

This map, indeed, shows that all Zn atoms form ZnO crystallites while the Ce atoms segregate in islands of CeO_2 joined to ZnO particles. On the contrary, the sample presents a good spatial dispersion of oxygen in both ZnO and CeO_2 crystals.

The chemical compositional analysis is very important to monitor the concentration of the dopant. The EDX analysis of the described samples (Table 2) shows that, as expected, only Zn and O are present in the non-doped sample of ZnO and that the total percentage of cerium in the doped sample is about 1.5%. The Ce/Zn molar ratio calculated from the atomic percentages is close to 1%, as expected from the nominal composition.

Table 2. Atomic percentage of elements obtained from EDX analysis

Sample	Elements	Atomic %	Ce/Zn ratio
ZnO	O	38.8	/
	Zn	61.2	
Ce-ZnO	O	35.7	0.94%
	Zn	62.8	
	Ce	1.5	

DRS UV-Vis analysis

We used the well-known TiO_2 P25 as reference sample for comparing the optical properties, surface area and, in particular, the photocatalytic efficiency. The optical spectra of the P25 sample and of bare and doped ZnO exhibit relatively small differences and confirm previous data reported in the literature [18]. Figure 4 shows the absorption spectra obtained for TiO_2 P25, ZnO and Ce-ZnO samples. As it can be seen the Ce doping of ZnO results in a very small increase in the overall absorption (see enlargement of Figure 4), towards the visible domain. The spectra are dominated by the valence band (VB) – conduction band (CB) transition occurring at about 400 nm (ca. 3 eV) for ZnO and Ce-ZnO, and at about 350 nm (ca. 3.5 eV) for P25.

Energy gap values have been calculated by linearization of the plot reporting $(\alpha h\nu)^{1/2}$ vs $h\nu$ typical of indirect band gap transitions for P25 and by linearization of the plot reporting $(\alpha h\nu)^2$ vs $h\nu$ typical of direct band gap transitions for ZnO and Ce-ZnO[19], results are reported in Table 3.

The calculated energy gap for the three samples are very as expected.

Table 3. Calculated energy gap (through the Tauc plot from DRS measures) and B.E.T. specific surface area (from nitrogen adsorption/desorption measures) of the samples.

Sample	E_g [eV]	S_{BET} [m^2/g]
P25	3.28	55
ZnO	3.26	<10
Ce-ZnO	3.27	<10

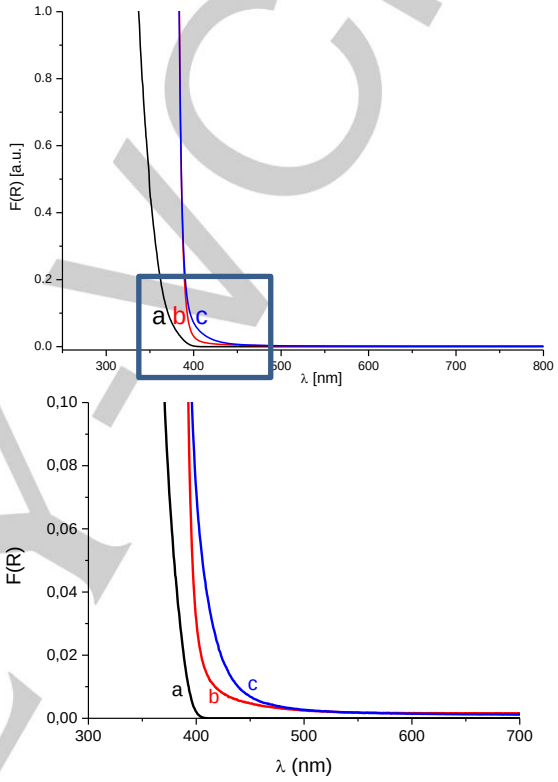

Figure 4. Absorption spectra of TiO_2 P25 (a), ZnO (b) and Ce-ZnO (c).

B.E.T. specific surface area

The specific surface area of the samples was measured applying the Brunauer–Emmett–Teller (B.E.T.) model on the N_2 adsorption measurement. The S_{BET} of the ZnO and Ce-ZnO samples results in a very low value, less than 10 m^2/g, compared to that of TiO_2 P25.

As it concerns the surface area we can just state that is low (less than 10 m^2/g) because of instrumental limits (N_2 adsorption is not fully reliable for systems having such a low area). Nevertheless such a low value is quite in agreement with the large values (> 150 nm) found with the XRD analysis.

The photocatalytic effect (see next paragraph) observed for the doped systems is due to the tiny shoulder indicating the presence of intra-band gap states and not to a real shift of the band gap itself.[4] We think that these intra-band gap states are

the responsible for the photocatalytic activity of the doped samples.

Photocatalytic performances

Degradation of phenol

Preliminary, we tested the behavior of bare and doped ZnO under UV-A irradiation in the photo-degradation of phenol, frequently used as probe molecule; for comparison purpose, P25 was employed as well. Direct photolysis and adsorption process in the dark are negligible. In a previous work [3], we explored the role of different dopant amounts and salt precursors on the catalyst efficiency and we concluded that the optimal dopant amount is fixed to 1%, while the best precursor salt was $CeCl_3$, due to favorable cerium oxidation state. Therefore, we produced our materials using these conditions but starting from two different zinc oxide precursors, namely zinc nitrate (ZnO) and zinc acetate (ZnOa).

Figure 5 shows the disappearance profiles for phenol over time in the presence of the synthetized materials and commercial TiO_2 P25. Interestingly, while the disappearance of the two molecules similarly occurred with both bare ZnO or commercial TiO_2 P25, the use of Cerium doped ZnO induced a sharp increase in the degradation of phenol. Doped zinc oxide prepared starting from nitrate salt (named ZnO-Ce) exhibits a higher activity than that synthetized via acetate precursor (named ZnOa-Ce). A possible explanation may lie in their different ability to produce a homogenous dispersion during the synthesis. In the presence of ZnO-Ce, phenol (P) is completely abated within 10 min of irradiation, while with ZnOa-Ce 30 min are required and even 60 min with P25. The early formed transformation products from phenol degradation are known to be catechol (Cat) and hydroquinone (HQ) [20] whose evolution profiles obtained using Ce-ZnO and TiO_2 are reported in the Figure 5 (bottom). When employing Ce-ZnO, HQ and Cat achieved the maxima concentration in few min and then they are easily degraded within 20 min of irradiation, so assessing that all aromatic compounds are completely abated. Conversely, with P25 their kinetic evolution are slowed down and up to 90 min are required. The performance of Ce-ZnO was also evaluated toward high phenol concentrations, aimed to test if this material is also suitable for the treatment of water with high content of organic pollutants. The photocatalytic degradation can be ascribed to a pseudo-first order kinetic model, so that the disappearance initial rate can be calculated by using mono-exponential decay, as described by the following equation:

$$C = C_0 e^{-kt}$$

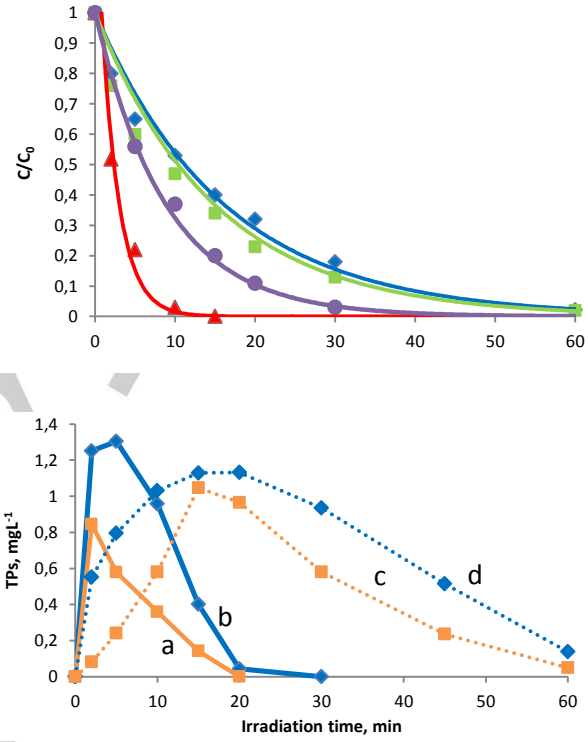

Figure 5. Phenol (10 mg/l) de gradation in the presence 1 g/l of bare ZnO (■) doped Ce-ZnO (▲),doped ZnOa-Ce (●) and P25 (♦) (top); (bottom) Transformation products formed following phenol degradation on Ce-ZnO and P25; (a) Cat Ce-ZnO, (b) HQ Ce-ZnO, (c) Cat P25, (d) HQ P25.

where C corresponds to pollutant concentration, k is the pseudo-first order kinetic constant, t is the reaction time and C_0 is pollutant concentration for t=0; the calculated pseudo-first order rate constants as a function of phenol concentration, as well as the half-lives ($t_{1/2}$), are plotted in Figure 6. Interestingly, when using Ce-ZnO phenol half-life time is reached within few minutes also when treating aqueous dispersion with high phenol content (i.e starting from 100 mg/L of phenol, 50% is degraded in 25 min), while with P25 half-life time increased up to 120 min.

By analyzing the initial rate in the different conditions, with P25 the rate level off for 60 mg/l of phenol, while with Ce-ZnO rate continues increasing up to 100 mg/L, so underlining that the

photoactivity of doped material remains still high also when treating concentrated aqueous solution of phenol, thus opening the door to its exploitation in the treatment of samples with high content of organic matter.

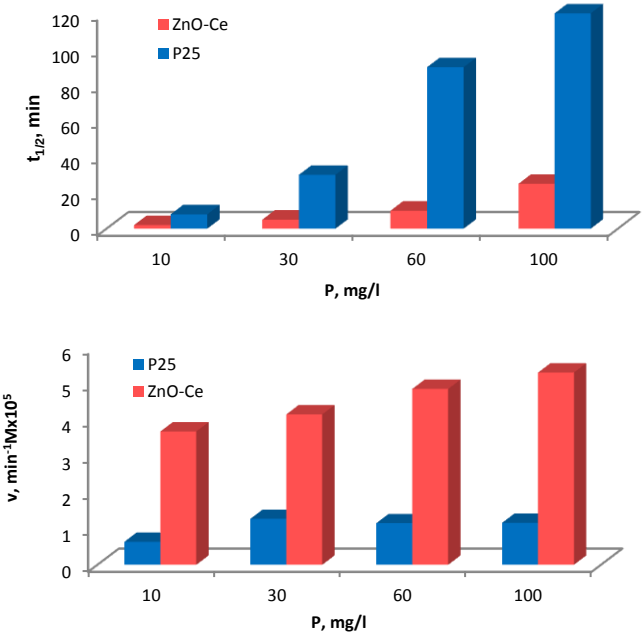

Figure 6. Phenol half-lives time (top) and rate (bottom) as a function of phenol (P) concentration in the presence of Ce-ZnO (■) and, for comparison, (■) P25 (1 g/l).

Degradation of X-ray contrast agents

The performance of ZnO and Ce-ZnO was also tested toward the photodegradation of some persistent iodinated X-ray contrast agents, namely iopamidol, iopromide and diatrizoate, three emerging contaminants known to be scarcely abated in the wastewater treatment plant [12]. The overall degradation curves for ICM are plotted in Figure 7, while the calculated initial rate constants are collected in Figure 8. Direct photolysis was assessed as blank experiment for all tested drug and, in all cases, was negligible. The employment of Ce-ZnO induced a strong increase in the degradation rate for all drugs. Considering iopamidol, its rate is 4 times higher when employing Ce-ZnO; half-life was shorten from 30 min (P25) to 2 min (Ce-ZnO) and the complete drug disappearance was achieved in only 30 min, while with P25 up to 4h are required.

A similar trend was observed with iopromide and diatrizoate, with a rate 3 times higher in the presence of Ce-ZnO and $t_{1/2}$ reduced from 40 (P25) to 15 min (Ce-ZnO) and from 2 h to 30 min, respectively; iopromide complete degradation was achieved within 2 h (Ce-ZnO) rather than 5 h (P25), while for diatrizoate degradation time passes from 16 h (P25) to 3h (Ce-ZnO).

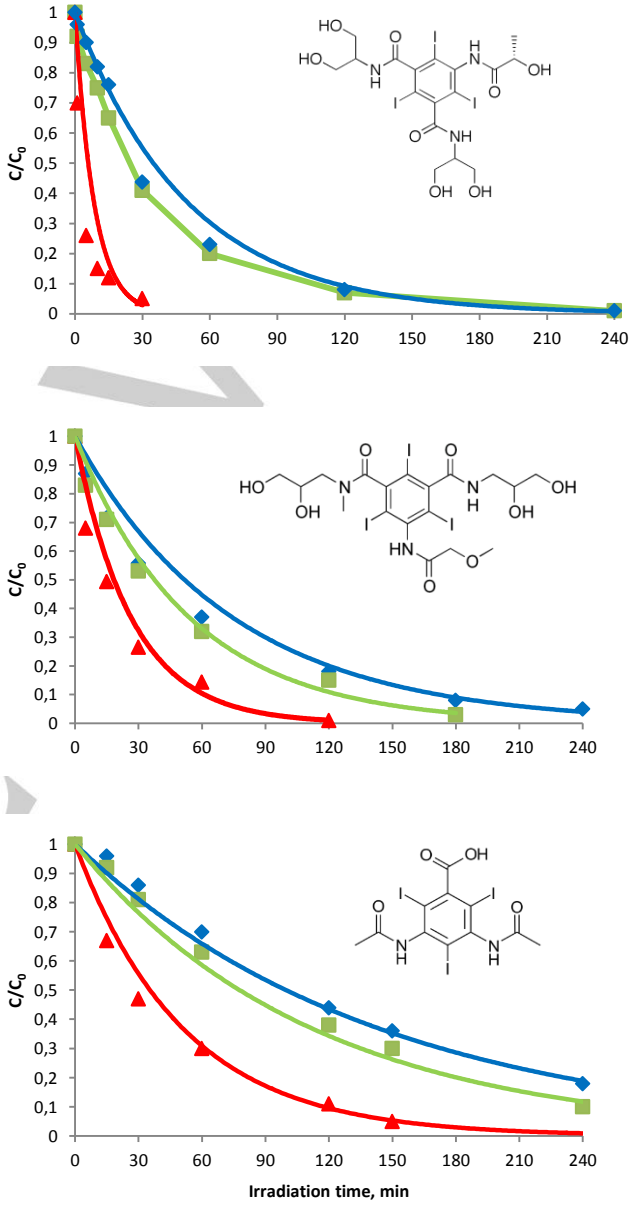

Figure 7. Iopamidol (top), iopromide (middle) and diatrizoate (bottom) (10 mg/l) degradation in the presence of bare ZnO (■) Ce-ZnO (▲) or (♦) P25 (1 g/l).

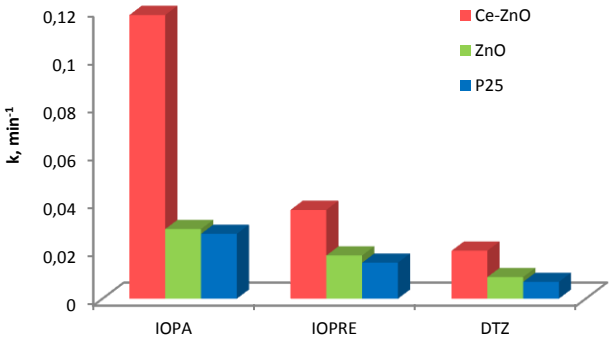

Figure 8. ICM constant rate in the presence of bare ZnO (■) Ce-ZnO (■) and (■) P25 (1 g/l).

We interpreted the higher photoactivity of the Ce-ZnO respect to the bare ZnO or to P25 in term of the role of intra band gap states generated in the doped material and in the interaction at the interfaces generated between ZnO crystallites with small amount of CeO_2 formed. Cerium, as most of the lanthanide, is stable in both the oxidation number +3 and +4 being the electronic configuration respectively $4f^1\ 6s^0$ and $4f^0\ 6s^0$, with the f orbitals close in energy to the other orbitals. F orbitals are mostly localized and less expanded respect to the d orbitals. These empty states (in the case of Ce^{4+}) act as a sort of link between the valence band and the conduction band of the oxide allowing low-energy photons to excite electrons from one band to the other. The mechanism, a sort of double jump photoexcitation, is analogous to that recently described by some of us to interpret the photocatalytic activity of N doped TiO_2 in visible light.[21] These factors, empty states as mid gap levels and junctions at the interfaces of different matrices, seem to be essential to ensure a certain efficiency to the two-photons excitation mechanism.

Conclusions

In this work we synthesized via hydrothermal process cerium doped zinc oxides. We used $CeCl_3$ as cerium precursor for the doping and the specific percentage of 1% molar of dopant has been selected as the most interesting according to the photocatalytic results obtained. The photocatalytic activity of the synthesized materials has been compared with the undoped material (bare ZnO) and with the benchmark TiO_2 P25 in the photodegradation of phenol used as probe molecule, at different concentrations. The obtained results of this preliminary screening were very encouraging. The synthesized material has been then tested also in the photodegradation of X-ray contrast agents, namely iopamidol, iopromide and diatrizoate, emerging contaminants known to be scarcely abated in the wastewater treatment plants. Also in this case the achievement of the complete drug disappearance in only 30 min was a great success especially if compared with the results present in the literature. ZnO doped with cerium chloride could represent an efficient candidate in the family of solar light photocatalysts.

Experimental Section

Materials

All reactants employed in this work were purchased from Aldrich and have purity higher than 99.9% and do not contain traces of lanthanides (except cerium salts). All reactants were used without any further purification treatment. Bare ZnO sample was synthesized starting from a 1M water solution of $Zn(NO_3)_2{\cdot}6H_2O$. Then a 4 M NaOH solution was added dropwise until the pH was 10-11, and finally the solution was transferred into a Teflon lined stainless steel 100mL autoclave (filling 70%), then treated at 175 °C overnight. The product was centrifuged and washed three times with deionized water, then dried at 70 °C. The Ce doped ZnO sample (Ce molar concentration 1%) was prepared adding the stoichiometric amount of $CeCl_3{\cdot}7H_2O$ in the starting solution, then the same procedure has been followed. The samples will be labeled as ZnO and Ce-ZnO.

TiO_2P25 Evonik was used as photocatalyst, after being subjectedtoirradiation andwashed withultrapure waterin order toeliminate the potential interference caused by adsorbed ions such as chloride,sulfate and sodium.

Phenol (P), catechol (CAT), hydroquinone (HQ), iopamidol (IOPA), iopromide (IOPRE), diatrizoate (DTZ), methanol (≥99.9%), acetonitrile (≥99.9%) and formicacid(99%) were purchased fromSigmaAldrich (Milan, Italy). HPLC grade water was from MilliQ System Academic (Waters, Millipore). HPLC grade methanol (BDH) and acetonitrile (Aldrich) were filtered through a 0.45 µm filter before use.

2.2 Materials characterization

Powder X-rays diffraction (XRD) patterns were recorded with a PANalytical PW3040/60 X'Pert PRO MPD using a copper K□ radiation source (0.15418 nm). The intensities were obtained in the 2θ ranges between 20° and 70°. The X'Pert High-Score software was used for data handling. Rietveld refinement was performed on the diffraction patterns to determine the crystallite size and relative abundance of phases, using the MAUD 2.26 software and a NIST Si powder to determine the instrumental function [17].

The TEM images were performed with a high-resolution analytical transmission microscope TEI Tecnai Orisis with an X-FEG Schottky field emitter (accelerating voltage 200 keV) equipped with Super-X EDX (Energy Dispersive X-ray) windowless detector system with 4-sector silicon drift detector (SDD) were used for sample imaging at the nanoscale. The Z-contrast images were acquired by means of a high angle annular dark field (HAADF) detector in the scanning transmission electron microscopy (STEM) mode. STEM images coupled with EDX elemental mapping were acquired with applied sample drift correction using Bruker Esprit software. Prior to microscopic analysis, the samples were ultrasonically dispersed in ethanol and dropped on a holey carbon film supported on a copper grid (Agar Scientific, 300 mesh).

The UV-Vis absorption spectra were recorded using a Varian Cary 5000 spectrometer, coupled with an integration sphere for diffuse reflectance studies (DRS), using a Carywin-UV/scan software. A sample of PTFE with 100% reflectance was used as reference.

The surface area measurements were carried out on a Micromeritics ASAP 2020/2010 using the Brunauer–Emmett–Teller (B.E.T.) model on the N_2 adsorption measurement. Prior to the adsorption run, all the samples were outgassed at 160 °C for 3 h. Size and shape of synthesized particles were determined through scanning electron microscopy by a Scanning Electron Microscope PhenomProX equipped with EDX analysis (Phenomworld).

Irradiation procedures

The irradiation experiments were carried out in Pyrex glass cells, filled with 5 ml of a suspension containing the analyte (20 mg/L) and the catalyst(1000 mg/L). Samples were subjected to different irradiation times (ranging from 5 min to 4 h), using a set of three TLK 40 W/05 (UV–Vis) fluorescent lamps (Phillips, Eindhoven, Nederland) with emission spectrum centered at 360 nm. The UV integrated irradiance on the cells in the 290–400 nm range wavelengths was 24 ± 1 W m^{-2} (measured with a CO.FO.MEGRA. (Milan, Italy) power-meter). The temperature reached during irradiation was 26 °C. After illumination, the entire content of each cell was filtered through a 0.45 μm filter and then analyzed. Photocatalytic activities of the catalysts (TiO_2-P25, bare ZnO, Cerium doped ZnO) were assessed through the photodegradation of phenol (P) and drugs under a variety of experimental conditions. Before irradiation, the suspensions were allowed to stay in the dark for 30 min under stirring, during which the solution concentration was monitored and adsorption equilibrium on the surface of the catalysts was reached. In all cases, adsorption on the catalyst surface was negligible. All experiments were performed in triplicate and we plotted the average value.

Analytical procedures

Liquid- Chromatography-UV

All compounds were monitored by using a Merck-Hitachi liquid chromatographer equipped with Rheodyne injector L-6200 and L-6200A pumps for high-pressure gradients, L-4200 UV-Vis detector (the detection wavelength was set at 240 nm) and a columnLiChrocart RP-C18 (Merck, 12,5 cm x 0,4 cm). Isocratic elution (1 mL/min flow rate) was carried out with 95% of phosphate buffer $1x10^{-2}$ M at pH 2.8 and 5% acetonitrile for IOPA and AC detection; in the case of IOPRE, 75/25 was used. Their retention times were 4.5 (IOPA), 3.0 (IOPRE) and 5.3 min (AC), respectively. The detectionwavelength was set at 240 nm. In thecaseofphenol, thedetectionwavelength was setat 220 nm; elution was carried out with80% ofphosphatebuffer $1x10^{-2}$ M at pH 2.8 and 20% acetonitrileandretentiontimes was 6.45 min.

Acknowledgements

We acknowledge support from a Marie Curie International Research Staff Exchange Scheme Fellowship (PHOTOMAT, proposalno. 318899) within the 7th European Community Framework Programme, project MAT4TREAT within the European Union's Horizon 2020 research and innovation programme under the Marie Skłodowska-Curie grant agreement No 645551 and the project funded by MIUR, in the frame of the collaborative international consortium WATERJPI2013-MOTREM of the Water Challenges for a Changing World Joint

Programming Initiative (WaterJPI) Pilot Call and the Local Funding of the University of Torino call_2014_L2_126. P.C and MC P. also acknowledge the Alfatest Strumentazione Scientifica srl for providing SEM pictures and Prof. Z. Sojka (Jagellonian University of Cracow) for the TEM images.

Keywords: iodinated X-ray contrast agents, zinc oxide, phenol, photocatalysis, cerium-doped

[1] F. Lu, W. Cai, Y. Zhang, *Adv. Funct. Mater.* **2008**, *18*, 1047-1056; S. Sakthivel, B. Neppolian, M. V. Shankar, B. Arabindoo, M. Palanichamy, V. Murugesan, *Sol. Energy Mater. Sol. Cells* **2003**, *77*, 65-82.

[2] C. Gionco, M. C. Paganini, M. Chiesa, S. Maurelli, S. Livraghi, E. Giamello, *Appl. Catal. A-Gen.* **2015**, *504*, 338-343.

[3] P. Calza, C. Gionco, M. Giletta, M. Kalaboka, V. A. Sakkas, T. Albanis, M. C. Paganini, *J. Hazard. Mater.* **2016**, In press.

[4] N. C. S. Selvam, J. J. Vijaya, L. J. Kennedy, *J. Nanosci. Nanotechnol.* **2014**, *14*, 2317-2324.

[5] K. G. Kanade, B. B. Kale, J. O. Baeg, S. M. Lee, C. W. Lee, S. J. Moon, H. J. Chang, *Mater. Chem. Phys.* **2007**, *102*, 98-104; C. Gionco, M. C. Paganini, E. Giamello, R. Burgess, C. Di Valentin, G. Pacchioni, *J. Phys. Chem. Lett.* **2014**, *5*, 447-451.

[6] M. Aslam, M. T. Qamar, M. T. Soomro, I. M. I. Ismail, N. Salah, T. Almeelbi, M. A. Gondal, A. Hameed, *Appl. Catal., B* **2016**, *180*, 391-402; J.-C. Sin, S.-M. Lam, K.-T. Lee, A. R. Mohamed, *J. Mol. Catal. A: Chem.* **2015**, *409*, 1-10.

[7] J. E. Drewes, P. Fox, M. Jekel, *J. Environ. Sci. Health., Part A* **2001**, *36*, 1633-1645; W. Seitz, J. Q. Jiang, W. H. Weber, B. J. Lloyd, M. Maier, D. Maier, *Environ. Chem.* **2006**, *3*, 35-39; R. L. Oulton, T. Kohn, D. M. Cwiertny, *J. Environ. Monit.* **2010**, *12*, 1956-1978; T. A. Ternes, R. Hirsch, *Environ. Sci. Technol.* **2000**, *34*, 2741-2748.

[8] T. Reemtsma, M. Jekel, *Organic Pollutants in the Water Cycle: Properties, Occurrence, Analysis and Environmental Relevance of Polar Compounds*, **2006**.

[9] M. E. Gale, A. H. Robbins, R. J. Hamburger, W. C. Widrich, *AJR Am J Roentgenol* **1984**, *142*, 333-335; H. D. Humes, D. A. Hunt, M. D. White, *Am. J. Physiol.* **1987**, *252*, F246-F255.

[10] J. L. Kormos, M. Schulz, H.-P. E. Kohler, T. A. Ternes, *Environ. Sci. Technol.* **2010**, *44*, 4998-5007; A. L. Batt, S. Kim, D. S. Aga, *Environ. Sci. Technol.* **2006**, *40*, 7367-7373.

[11] W. Kalsch, *Sci. Total Environ.* **1999**, *225*, 143-153; A. Haiss, K. Kummerer, *Chemosphere* **2006**, *62*, 294-302.

[12] P. Westerhoff, Y. Yoon, S. Snyder, E. Wert, *Environ. Sci. Technol.* **2005**, *39*, 6649-6663.

[13] G. Del Moro, C. Pastore, C. Di Iaconi, G. Mascolo, *Sci. Total Environ.* **2015**, *506*, 631-643.

[14] R. R. Singh, Y. Lester, K. G. Linden, N. G. Love, G. E. Atilla-Gokcumen, D. S. Aga, *Environ. Sci. Technol.* **2015**, *49*, 2983-2990.

[15] T. E. Doll, F. H. Frimmel, *Catal. Today* **2005**, *101*, 195-202; T. E. Doll, F. H. Frimmel, *Water Res.* **2005**, *39*, 847-854; T. E. Doll, F. H. Frimmel, *Water Res.* **2004**, *38*, 955-964.

[16] M. N. Sugihara, D. Moeller, T. Paul, T. J. Strathmann, *Appl. Catal., B* **2013**, *129*, 114-122; S. Carbonaro, M. N. Sugihara, T. J. Strathmann, *Appl. Catal., B* **2013**, *129*, 1-12.

[17] L. Lutterotti, *Nucl. Instrum. Methods Phys. Res., Sect. B* **2010**, *268*, 334-340.

[18] M. Rezaei, A. Habibi-Yangjeh, *Mater. Lett.* **2013**, *110*, 53-56.

[19] G. Martra, E. Gianotti, S. Coluccia, in *Metal Oxide Catalysis*, Wiley-VCH Verlag GmbH & Co. KGaA, **2009**, pp. 51-94.

[20] C. Minero, G. Mariella, V. Maurino, E. Pelizzetti, *Langmuir* **2000**, *16*, 2632-2641; Z. Guo, R. Ma, G. Li, *Chem. Eng. J.* **2006**, *119*, 55-59.

[21] G. Barolo, S. Livraghi, M. Chiesa, M. C. Paganini, E. Giamello, *J. Phys. Chem. C* **2012**, *116*, 20887-20894.

WILEY-VCH

Entry for the Table of Contents (Please choose one layout)

Layout 1:

FULL PAPER

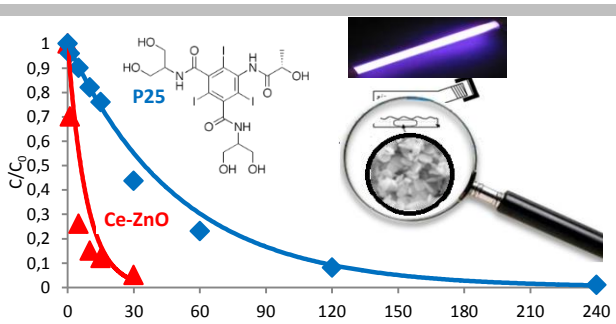

Text for Table of Contents

*Author(s), Corresponding Author(s)**

Page No. – Page No.

Title

Layout 2:

FULL PAPER

((Insert TOC Graphic here; max. width: 11.5 cm; max. height: 2.5 cm))

*Author(s), Corresponding Author(s)**

Page No. – Page No.

Title

Text for Table of Contents

WILEY-VCH